Journal of
Analytical & Bioanalytical Techniques

Grilj et al., J Anal Bioanal Tech 2014, S12
DOI: 10.4172/2155-9872.S12-005

Research Article Open Access

A Beamline for Time-Resolved Extreme Ultraviolet and Soft X-Ray Spectroscopy

Jakob Grilj[1,2], Emily Sistrunk[1], Markus Koch[1,3] and Markus Gühr[1]*

[1]*Stanford PULSE Institute, SLAC National Accelerator Laboratory, Menlo Park, USA*
[2]*Laboratoire de Spectroscopie Ultrarapide, Ecole Polytechnique Federale de Lausanne EPFL, Switzerland*
[3]*Institute of Experimental Physics, Graz University of Technology, Austria*

Abstract

High harmonic generation is a convenient way to obtain extreme ultraviolet light from table-top laser systems and the experimental tools to exploit this simple and powerful light source for time-resolved spectroscopy are being developed by several groups. For these applications, brightness and stability of the high harmonic generation is a key feature. This article focuses on practical aspects in the generation of extreme ultraviolet pulses with ultrafast commercial lasers, namely generation parameters and online monitoring as well as analysis of generation yield and stability.

Keywords: High harmonic generation; Extreme ultraviolet; Soft v-ray; Ultrafast spectroscopy; High harmonic yield

Introduction

The interaction of light with the valence electrons of molecules and materials presents a central problem for the understanding of life and many technological applications. Vision and light harvesting involve the transfer of light energy into chemical energy [1-3], the photoprotection of DNA and its components involves the selective transfer of light energy into heat instead of chemical change [4,5]. Materials that change their properties upon light illumination [6-8] as well as photovoltaic systems [9] promise major technological breakthroughs. The photoexcited state of matter is generally described by a complex concerted motion of electrons and nuclei on the timescale of femto- to picoseconds, whose understanding is still challenging [10] demanding extensive experimental studies. The invention of ultrafast lasers has opened this timescale for direct investigations [11].

Due to the recent progress in strong field laser interactions, femto- and attosecond light pulses in the extreme ultraviolet (EUV) spectral range between 10 and 100 eV photon energy are becoming more widespread in ultrafast laser laboratories. Similar to x-rays, the photons in the EUV spectral domain interact preferentially with atomic core levels, which are genuinely distinct for different chemical elements. Together with the relatively tight spatial extend of the corresponding core wave function, the EUV pulses are used for spatially and element selective spectroscopy of matter. The most important core levels in the EUV spectral domain are the 3p and 4p states of the 3d and 4d transition metals [12]. Pioneering time resolved studies using EUV probe pulses were performed in atoms and molecules [13,14] as well as on materials [15-19] and have recently also been extended to solvated systems [20].

The generation mechanism for the EUV pulses is based on the sub-optical cycle interaction of a strong infrared (IR) laser field with a rare gas target, which is generally called high harmonic generation (HHG). During one optical half-cycle, part of the valence electrons is ionized from an atom. The electron gains kinetic energy in the IR field which can be transferred into photon energy upon inelastic collision of the electron with the remaining ion [21-23]. The small cross section for this single atom inelastic collision process can only partially be compensated by coherent phase matching over the excitation medium. Unlike light from other nonlinear processes, the HHG-EUV light carries an intensity dependent phase, making phase matching much more demanding [24-26]. Popular schemes to make use of some phase matching include gas jets [27-29], gas cells [16,30-34] multiple gas cells in series [35] hollow core capillaries [36] and plasma plumes [37].

Femotosecond EUV and soft x-ray (SXR) light pulses can also be generated in synchrotrons in a so called slicing beam line [38] which can deliver sub-picosecond time resolution though at largely reduced flux compared to normal operation. Despite the experimental challenges, they have been successfully used to elucidate photochemical reactions [39]. The free electron lasers (FEL) FLASH and Fermi@Elettra can generate femtosecond EUV light pulses. Fermi@Elettra is seeded by an external laser with UV light but seeding with shorter wavelength pulses from a HHG source is envisaged [40] and has been successfully demonstrated in a test facility at Spring 8 [41].

In this paper, we present a beamline for optimal transmission of the EUV light while filtering the strong infrared field. We present a simple yet effective online monitor for the relative intensity of the EUV light, which allows us to optimize and monitor the HHG efficiency. The device is based on a grazing incidence mirror for the EUV pulses. We present our approach of optimizing the HHG process in a gas cell and present systematic variations with cell length, target gas pressure and position with respect to the focal spot of the IR driver pulse. The beamline can be conveniently coupled to an optical excitation pulse for realizing time resolved absorption, photoemission and transient grating techniques.

Experimental Set-up and Optical Components

A scheme of the set-up is shown in Figure 1. It is based on an amplified laser system delivering 8 mJ 25fs pulses with a center

***Corresponding author:** Markus Gühr, Stanford PULSE Institute, SLAC National Accelerator Laboratory, Menlo Park, CA 94025, USA, Tel: +1 650 926 5550; Fax: +1 650 926 3712; E-mail: mguehr@slac.stanford.edu

Received December 19, 2013; **Accepted** January 25, 2014; **Published** January 28, 2014

Citation: Grilj J, Sistrunk E, Koch M, Gühr M (2014) A Beamline for Time-Resolved Extreme Ultraviolet and Soft X-Ray Spectroscopy. J Anal Bioanal Tech S12: 005. doi:10.4172/2155-9872.S12-005

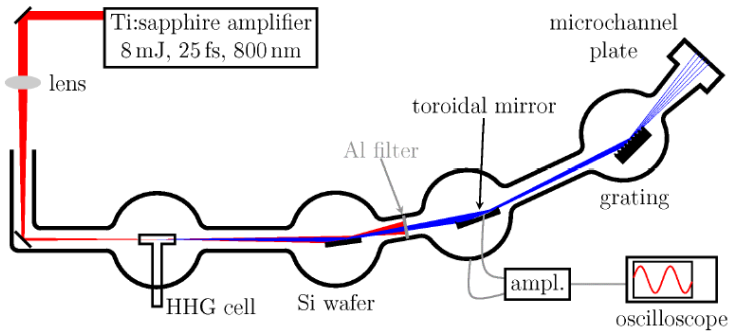

Figure 1: Experimental set-up. The 800 nm laser beam is focused into the HHG cell with a long focal length, free to move lens, generating EUV light through HHG. The 800 nm light is removed by a combination of Si wafer and Al filter. For this study the EUV light is spectrally dispersed onto the detector while for pump-probe studies, a sample (photoexcited by a fraction of the IR pulse) would reside at the focus of the toroidal mirror. The efficiency and stability of the EUV can be monitored on an oscilloscope.

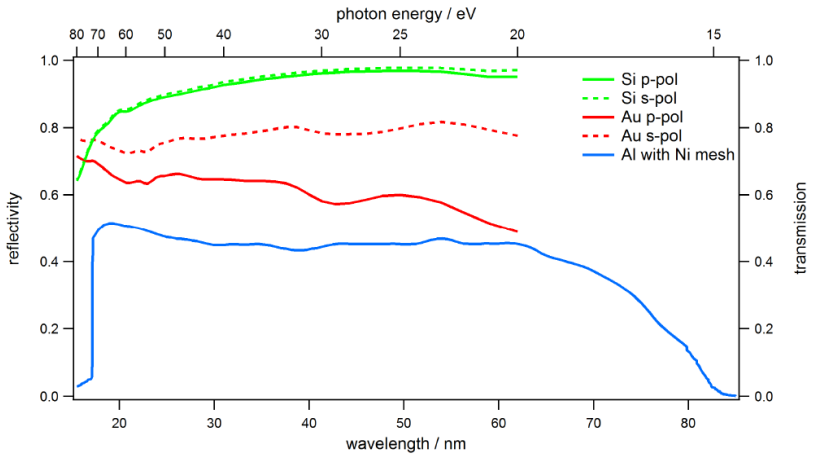

Figure 2: Calculated (see text) reflectivity of silicon (AOI=85 degrees) and gold (AOI 82.5 degrees) and measured [57] transmittance of a 150 nm thick aluminum foil (AOI=0 degrees;).

wavelength of 800 nm at 1 kHz repetition rate. About 4.5 mJ (peak power 2×10^{11} W) are used in the high harmonic generation (HHG), the remainder can serve for pump-probe experiments (not shown). The beam that drives the HHG is focused into the vacuum chamber by a lens of f=2270 mm or f=1680 mm at 800 nm. Care is taken that the beam diameter at the entrance port of the HHG chamber is sufficiently large to avoid beam profile deterioration due to nonlinear effects in the quartz window. The exact position of the focus can be altered by moving the lens.

The T-shaped HHG cell is machined from aluminum rod of varying length and contains a gas column of 4.4 mm diameter. The cell ends are capped with 100 μm thick copper or aluminum foil which is perforated by the laser. Hence the cell does not need to be precision aligned to the laser, but the foils are exchanged on a regular basis. The gas inlet is at the center of the cell where the backing pressure is controlled by a fine dosing valve. The backing pressure of the cell is about 10 torr. A turbo molecular pump with ~1600 liters/s pump speed keeps the vacuum around 10^{-3} torr in the chamber containing the gas cell leaking through the laser drilled holes. The cell also generates high harmonics if not sealed (at slightly higher pressures and roughly 5 times lower efficiency) which is convenient for alignment purposes. In that case, the cutoff harmonic is lower by about 10 eV under comparable parameters.

After the HHG cell, the 800 nm laser fundamental and EUV light propagate collinearly in vacuum. Separation of EUV light from the IR is achieved by a Si mirror [42,43] on which they are incident at an angle of 85 degrees to the surface normal, close to Brewster angle of 75 degrees for 800 nm. Thereby a major amount of the ~10^6 times stronger fundamental is removed from the EUV beam path. A 150 nm thick aluminum foil (purchased either from Luxel or Lebow) serves as filter for the IR light reflected off of the silicon mirror. Without the Si mirror, the Al filter would be destroyed by the intense fundamental beam.

The EUV light is refocused by a toroidal gold mirror (f=650 mm) with a tangential radius of curvature of 9194 mm and a saggital radius of curvature of 156.6 mm, at which the light is incident at an angle of incidence AOI=82.5 degrees to the surface normal. In studies of molecular dynamics, the sample sits at the focal spot of the toroidal mirror and the probe light is dispersed by a spectrometer (not shown). Figure 1 shows a spectrometer set-up in which the toroidal mirror is used in combination with a flat grating to characterize the HHG source. The gold grating (Edmund optics, 830 lines/mm, blazing angle 19.38 degrees, AOI=70 degrees) is placed downstream from the toroidal mirror to spectrally disperse the EUV light onto a micro channel plate (MCP)/phosphor screen detector and record on a charge coupled device (CCD). We rotate the grating to display different sections of the spectrum which heavily distorts the aspect of the spectra.

The reflectance of silicon and gold at the respective AOI and polarization have been calculated based on the data of Palik [44] and are represented in Figure 2. Since the EUV reflectivity drops rapidly when the AOI at the silicon mirror approaches the Brewster angle for 800 nm, the AOI chosen is a compromise between suppressing the unwanted IR and extinguishing the EUV light. As can be seen in Figure 2, the reflectance of both, Au and Si, is higher for s-polarized EUV light especially in the photon energy range of a few tens of eV. Yet, only at p-polarization the Brewster condition can be exploited to suppress the IR. Since the HHG polarization is identical to that of the IR, we need to operate the beamline with p-polarized EUV light.

The 20 to 70 eV transmittance window of an ideal 150 nm Al aluminum foil shown in Figure 2 is valid in the absence of surface oxidation but takes into account that the transmission is lowered by 25% for filters supported by a nickel mesh. Surface oxidation can be modeled as a 3 nm thick Al_2O_3 layer on each surface which reduces the transmittance to 40 to 70% in the 30 to 70 eV spectral range [45]. In practice, the losses on the filtering and refocusing optics are ca. 90% in the 20 to 70 eV range with steep increases on both the low and high energy side.

The grazing incidence angles on the optics required when using EUV light make the beamline relatively long. Even in the compact set-up shown in Figure 1, the focal spot of the toroidal mirror (the position of the sample in time-resolved experiments) is at a distance of roughly 9 m from the amplified laser system. A good temperature stability of the laboratory is thus important to avoid the pump and probe beams to walk off during an experiment.

Online Monitoring of HHG

The toroidal mirror has a reflectivity of 50-60% for p-polarized EUV radiation in the spectral region of interest and at the angle of incidence used in our set-up. The 40% of the light which is not reflected is absorbed and partially causes emission of photoelectrons from the gold surface. We use the photocurrent to measure the overall yield and monitor the stability of HHG during experiments. To this end, we measure for each pulse the drain current flowing from the mirror to ground through an amplifier (SRS low noise charge sensitive amplifier model SR570 with a 6 db 1 kHz band pass filter and a sensitivity of 2 nA/V). This way of monitoring the HH radiation does not require adding elements to the beam path, and can be conveniently implemented in any set-up that uses an electrically conducting reflective element for the EUV. We use the device as online tool to access total HHG efficiency and stability without adding losses in the beam line.

Figure 3 shows the gold mirror, which is contacted at its edge via a copper foil. The right part of Figure 3 shows a representative reading from the oscilloscope. The integral over the positive part of the signal corresponds to the charge drawn for each laser pulse. The negative part stems from ringing of the amplifier. When interfaced with a computer, a single shot analysis of the HH flux is possible with this method. The noise is determined by the amplification process and can be estimated from the signal in the absence of EUV radiation. For the configuration in our lab, the error is on the order of 1%.

The yield of photoelectron ejection from a thick gold layer in the EUV region has been documented [46]. Assuming unity detection efficiency and taking a typical reading of 5×10^{-13} Coulomb on the HH monitor tool, we calculate an integrated flux of 10^8 photons per laser pulse in the whole spectrum impinging on the gold mirror. This yields a lower limit of 4×10^{-7} for the conversion efficiency in the HHG cell for each harmonic in the 20 to 35 eV energy range when considering the reflectivity and transmission of the optics in the EUV beam path. In a pump-probe set-up, 10^7 EUV photons arrive at the sample per laser pulse.

In a typical experiment, the yield of HH drops to ca. 70% its initial value during the first 12 hours, and then remains stable for several days. Exchanging the copper plates restores the initial yield. With the tool described here, the EUV flux can be monitored while performing pump-probe experiments and used to correct for shot-to-shot noise and long term drifts, which greatly enhances the sensitivity of pump-probe measurements.

High Harmonic Generation

A spectrum of the high harmonics is shown in Figure 4. The wavelength dependent reflectivity of the grating used to disperse the spectrum is not known so the spectrum is not corrected for this effect. A flat gold surface has an EUV reflectivity of 5% at this angle (that would correspond to the zero order of the grating), rather independent of the exact photon energy.

The harmonics are identified by their separation on the screen and the calculated dispersion angles. It is remarkable that the 11th harmonic at 77 nm is present in the spectrum although the transmittance of the Al filter at this wavelength is low. This is due to the higher conversion efficiency towards lower harmonics, as they are closer to the perturbative domain of harmonic generation. At the high energy side, the spectrum is limited by the harmonic cutoff which is lower than expected due to an astigmatic beam profile at the HHG cell, resulting in lower intensity compared to a perfect Gaussian mode.

The yield of EUV radiation is determined by three important parameters: i) the length of the generation medium L_{med}; ii) the coherence length L_{coh}, i.e. the length over which the light generated by

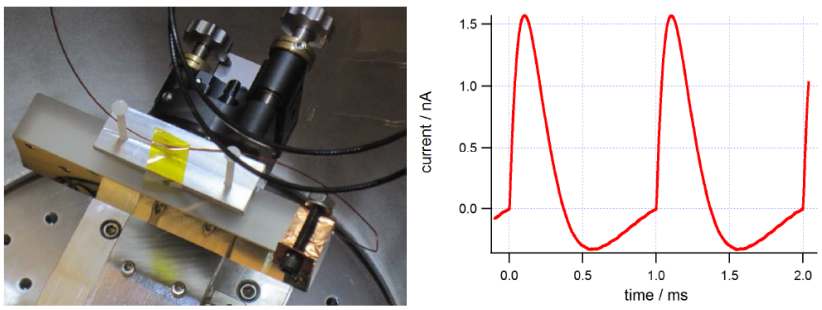

Figure 3: Left: Au mirror contacted by a copper sheet to measure the photocurrent. Right: High Harmonic Monitor reading on the oscilloscope. An integration over the scope trace results in the integrated charge from a single EUV pulse.

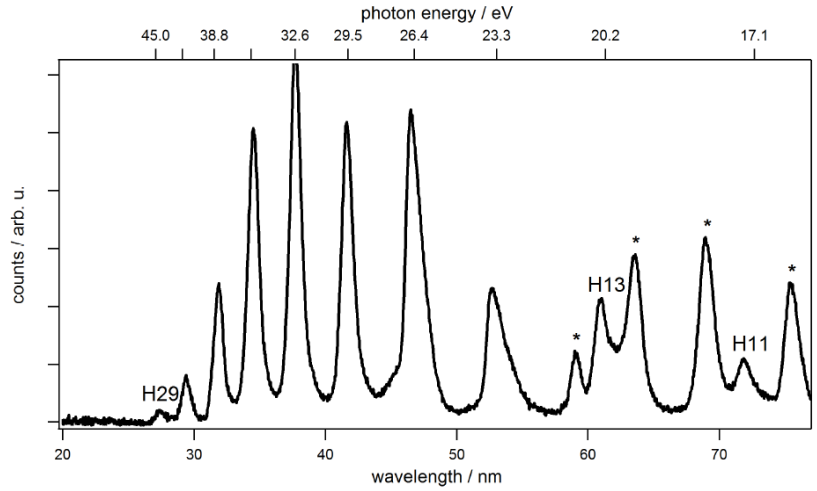

Figure 4: Spectrum of the high harmonics generated in a 60 mm long cell with Ar at I_{laser}=1.3•10^{14} W/cm^2 (f=1680 mm). The peaks marked with asterisks are assigned to 2nd order reflection of the grating. The spectrum is not corrected for the grating reflectivity and detector response.

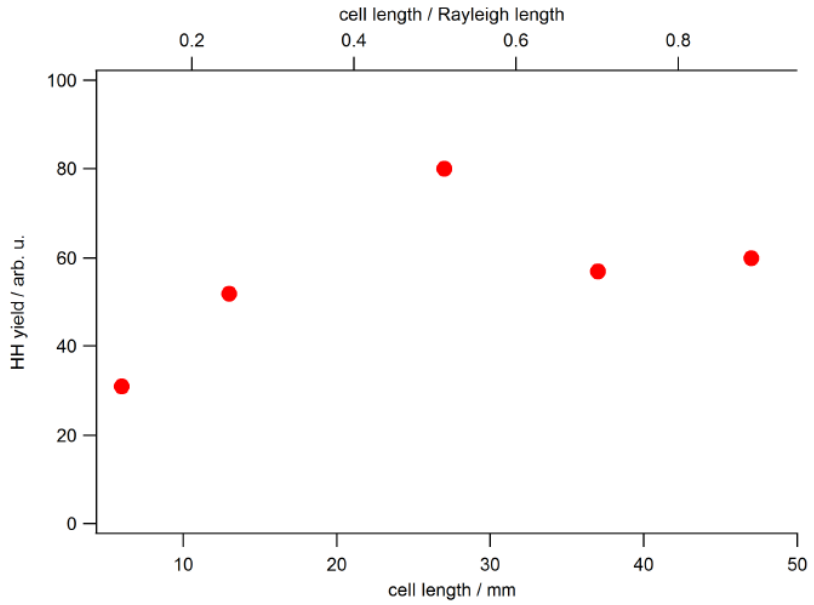

Figure 5: Efficiency of HHG in argon as a function of HHG cell length. I_{laser} = 6•10^{13} W/cm^2, f=2270 mm. The rise and decay is in qualitative agreement with a theoretical model in Ref. 48 assuming an absorption length in the few mm to cm regime.

the individual emitters interferes constructively; and iii) the absorption length L_{abs}, i.e. the length over which the intensity of the EUV radiation decreases to e^{-1} due to absorption by the medium [47]. The coherence and the absorption length is wavelength dependent.

The coherence length is determined by the phase mismatch between fundamental and high harmonics. Prominent factors for the mismatch are the intensity dependent dipole phase $\phi(I)$ of the harmonics as well as dispersion from the neutral medium and plasma and the so-called Gouy phase shift. Owing to the effect of $\phi(I)$ and the Gouy phase, a focus position before the generation medium enhances the HH yield [24-26,28]. Loose focusing or propagation inside a waveguide reduces the importance of $\phi(I)$ and the Gouy phase such that dispersion and absorption become important [48,49].

The absorption length L_{abs} is a function of medium density, hence the pressure inside the generation cell. Like other groups [50-52], we find the HH yield to reach a plateau which, in the case of our cell design, is reached at backing pressures of a few torr. No influence of medium temperature on the HHG process has been reported and it can be expected to be small since the process takes place in a plasma.

From a simplified one dimensional model, optimal yield is predicted for $L_{coh}>5\times L_{abs}$ and $L_{med}>3\times L_{abs}$ [48]. Shorter media do not allow for a coherent build-up of intensity while for longer cell lengths absorption diminishes the conversion efficiency as the IR beam loses intensity with propagation. Even at the unphysical assumption of infinite coherence length, the yield saturates due to absorption. At the parameters given before, the efficiency reaches half of that asymptotic value [48].

In practice, phase matching is accomplished by adjusting the length and density of the generation medium, the driving laser intensity, focal length and focus position such as to maximize the flux for the photon energy range of interest [47,52].

Takahashi et al. and Midorikawa et al. [52,53] as well as He et al. [54] studied the influence of cell length on the HH yield in a loose focusing geometry and with cells of several centimeter length. In addition they examined the quality and divergence of the emitted HH beam. Systematic studies of HHG parameters in a single cell have also been reported by Ditmire et al. [28] using thin cells (<1 mm) and Seres et al. [35] using multiple cells.

We determined the influence of medium length for the f=2260 mm lens. Figure 5 shows the overall yield of HHG in argon, as obtained from the HH monitor tool, for cells with a length varying from 6 to 47 mm. For the data summarized in Figure 5, all other parameters (gas pressure, laser pulse chirp, position of the focus with respect to the cell center) were optimized for overall HH yield for each cell. As expected, the yield changes significantly with cell length and shows a maximum when it approaches half the Rayleigh length, which equals 52.6 mm (28.8) for the lens with a focal length of f=2270 mm (1680 mm). There is a steep increase below this optimum length while the yield levels off at longer cell lengths.

For a pressure of 10 torr, the absorption length L_{abs} in argon ranges from 1 mm (H11) to 30 mm (H29) for the harmonics present in the spectrum shown in Figure 4 [55]. Comparing Figure 5 with a one dimensional model [48], we can infer that the coherence length L_{coh} in this setup is close to $5\times L_{abs}$ since the experimental data reproduces both, the rise and slight decay of efficiency depicted in Figure 1 in Ref [48]. Indeed, Labs is reasonably close to 1/3 of the cell length for the dominant harmonics. Moreover, we find our results to be in line with those of Takahashi et al. [52] and similar to the parameters used by Wernet et al. [33] or He et al. [54].

Outlook

Ultrafast time-resolved electronic spectroscopy in the EUV spectral region is capable of unprecedented temporal and spectral resolution and makes the complete dynamics of any molecular system traceable. The information gain will facilitate the interpretation of complex transient spectra. Electron correlation effects well known from steady-state techniques can be followed in real-time.

High harmonic generation can deliver ultra-short laser pulses of high coherence and low divergence in this spectral range with table-top commercial equipment. While many proof-of-principle experiments have already shown the applicability of HHG as EUV light source in ultrafast experiments, substantial improvements in photon flux and stability are necessary for a more routine use. Transient absorption is a photon hungry technique that requires probe light of high brightness and stability. Photoelectron detection does not need high pulse energies but benefits from high repetition rate sources. Naturally, a high photon flux is imperative for multiphoton and multidimensional spectroscopies, the latter of which are yet to be demonstrated at such short wavelengths.

Finally, the techniques are about to conquer after the gaseous and solid phase also the liquid phase which is most relevant for chemistry [20,56,57].

Acknowledgements

J. G. would like to acknowledge support by the European Research Agency via the FP-7 PEOPLE Program (Marie Curie Action 298210). M.K. acknowledges funding from the Austrian Science Fund (FWF, Erwin Schrodinger Fellowship, J 3299-N20). M. G. acknowledges funding via the Office of Science Early Career Research Program through the Office of Basic Energy Sciences, U.S. Department of Energy. This work was supported by the AMOS program within the Chemical Sciences, Geosciences, and Biosciences Division of the Office of Basic Energy Sciences, Office of Science, U.S. Department of Energy.

References

1. Peteanu LA, Schoenlein RW, Wang Q, Mathies RA, Shank CV (1993) The first step in vision occurs in femtoseconds: complete blue and red spectral studies. Proc Natl Acad Sci USA 90: 11762-11766.
2. Prokhorenko VI, Nagy AM, Waschuk SA, Brown LS, Birge RR, et al. (2006) Coherent control of retinal isomerization in bacteriorhodopsin. Science 313: 1257-1261.
3. Polli D, Altoè P, Weingart O, Spillane KM, Manzoni C, et al. (2010) Conical intersection dynamics of the primary photoisomerization event in vision. Nature 467: 440-443.
4. Crespo-Hernández CE, Cohen B, Hare PM, Kohler B (2004) Ultrafast excited-state dynamics in nucleic acids. Chem Rev 104: 1977-2019.
5. Middleton CT, de La Harpe K, Su C, Law YK, Crespo-Hernández CE, et al. (2009) DNA excited-state dynamics: from single bases to the double helix. Annu Rev Phys Chem 60: 217-239.
6. Bigot J-Y, Vomir M, Beaurepaire E (2009) Coherent ultrafast magnetism induced by femtosecond laser pulses. Nat Phys 5: 515-520.
7. Jerominek H, Vincent D, Picard F (2099) Vanadium oxide films for optical switching and detection. Opt Eng 32: 2092-2099.
8. Irie M (2000) Diarylethenes for Memories and Switches. Chem Rev 100: 1685-1716.
9. Grätzel M (2009) Recent advances in sensitized mesoscopic solar cells. Acc Chem Res 42: 1788-1798.
10. Plasser F, Barbatti M, Aquino AJA, Lischka H (2012) Electronically excited states and photodynamics: a continuing challenge. Theor Chem Acc 131: 1073.
11. Zewail A (2000) Femtochemistry: Atomic-Scale Dynamics of the Chemical Bond. J Phys Chem A 104: 5660-5694.
12. Henke BL, Gullikson EM, Davis JC (1993) X-Ray Interactions: Photoabsorption, Scattering, Transmission, and Reflection at *E*=50-30,000 eV, *Z*=1-92. At Data Nucl Data Tables 54: 181-342.
13. Loh ZH, Khalil M, Correa RE, Santra R, Buth C, et al. (2007) Quantum state-resolved probing of strong-field-ionized xenon atoms using femtosecond high-order harmonic transient absorption spectroscopy. Phys Rev Lett 98: 143601.
14. Loh ZH, Leone SR (2008) Ultrafast strong-field dissociative ionization dynamics of CH2Br2 probed by femtosecond soft X-ray transient absorption spectroscopy. J Chem Phys 128: 204302.
15. Bauer M, Lei C, Read K, Tobey R, Gland J, et al. (2001) Direct Observation of Surface Chemistry Using Ultrafast Soft-X-Ray Pulses. Phys Rev Lett 87: 025501.
16. Bauer M (2005) Femtosecond ultraviolet photoelectron spectroscopy of ultrafast surface processes. J Phys Appl Phys 38: R253-R267.
17. La-O-Vorakiat C, Siemens M, Murnane MM, Kapteyn HC, Mathias S, et al. (2009) Ultrafast demagnetization dynamics at the M edges of magnetic elements observed using a tabletop high-harmonic soft X-ray source. Phys Rev Lett 103: 257402.
18. Dakovski GL, Li Y, Durakiewicz T, Rodriguez G (2010) Tunable ultrafast extreme ultraviolet source for time- and angle-resolved photoemission spectroscopy. Rev Sci Instrum 81: 073108.
19. Vura-Weis J, Jiang C-M, Liu C, Gao H, Lucas JM, et al. (2013) Femtosecond $M_{2,3}$-Edge Spectroscopy of Transition-Metal Oxides: Photoinduced Oxidation State Change in α-Fe_2O_3. J Phys Chem Lett 4: 3667-3671.
20. Faubel M, Siefermann KR, Liu Y, Abel B (2012) Ultrafast soft X-ray photoelectron spectroscopy at liquid water microjets. Acc Chem Res 45: 120-130.
21. Krause JL, Schafer KJ, Kulander KC (1992) High-order harmonic generation from atoms and ions in the high intensity regime. Phys Rev Lett 68: 3535-3538.
22. Schafer KJ, Yang B, DiMauro LF, Kulander KC (1993) Above threshold ionization beyond the high harmonic cutoff. Phys Rev Lett 70: 1599-1602.

23. Ivanov MY, Corkum PB (1993) Generation of high-order harmonics from inertially confined molecular ions. Phys Rev A 48: 580-590.

24. Salieres P, Ditmire T, Perry MD, l'Huillier A, Lewenstein M (1996) Angular distributions of high-order harmonics generated by a femtosecond laser. J Phys B 29: 4771-4786.

25. Balcou P, Salieres P, l'Huillier A, Lewenstein M (1997) Generalized phase-matching conditions for high harmonics: The role of field-gradient forces. Phys Rev At Mol Opt Phys 55: 3204-3210.

26. Gaarde MB, Tate JL, Schafer KJ (2008) Macroscopic aspects of attosecond pulse generation" Invited Topical Review. J Phys B 41: 2001.

27. McPherson A, Gibson G, Jara H, Johann U, Luk TS, et al. (1987) Studies of multiphoton production of vacuum-ultraviolet radiation in the rare gases. J Opt Soc Am B 4: 595-601.

28. Ditmire T, Crane JK, Nguyen H, DaSilva LB, Perry MD (1995) Energy-yield and conversion-efficiency measurements of high-order harmonic radiation. Phys Rev A 51: R902-902R905.

29. Schmidt BE, Shiner AD, Giguère M, Lassonde P, Trallero-Herrero CA, et al. (2012) High harmonic generation with long-wavelength few-cycle laser pulses. J Phys B At Mol Opt Phys 45: 074008.

30. Spielmann Ch, Burnett NH, Sartania S, Koppitsch R, Schnürer M, et al. (1997) Generation of Coherent X-rays in the Water Window Using 5-Femtosecond Laser Pulses. Science 278: 661-664.

31. Farrell JP, McFarland BK, Gühr M, Bucksbaum PH (2009) Relation of high harmonic spectra to electronic structure in N_2. Chem Phys 366: 15-21.

32. Farrell JP, Petretti S, Förster J, McFarland BK, Spector LS, et al. (2011) Strong field ionization to multiple electronic states in water. Phys Rev Lett 107: 083001.

33. Wernet P, Gaudin J, Godehusen K, Schwarzkopf O, Eberhardt W (2011) Femtosecond time-resolved photoelectron spectroscopy with a vacuum-ultraviolet photon source based on laser high-order harmonic generation. Rev Sci Instrum 82: 063114.

34. Frank F, Arrell C, Witting T, Okell WA, McKenna J, et al. (2012) Invited review article: technology for attosecond science. Rev Sci Instrum 83: 071101.

35. Seres J, Yakovlev VS, Seres E, Streli C, Wobrauschek P, et al. (2007) Coherent superposition of laser-driven soft-X-ray harmonics from successive sources. Nat Phys 3: 878-883.

36. Popmintchev T, Chen MC, Popmintchev D, Arpin P, Brown S, et al. (2012) Bright coherent ultrahigh harmonics in the keV x-ray regime from mid-infrared femtosecond lasers. Science 336: 1287-1291.

37. Ganeev RA (2012) High-order harmonic generation in laser plasma: Recent achievements. Laser Phys 22: 1177-1188.

38. Schoenlein RW, Chattopadhyay S, Chong HH, Glover TE, Heimann PA, et al. (2000) Generation of femtosecond pulses of synchrotron radiation Science 287: 2237-2240.

39. Bressler C, Chergui M (2010) Molecular structural dynamics probed by ultrafast X-ray absorption spectroscopy. Annu Rev Phys Chem 61: 263-282.

40. Goh SJ, van der Slot PJM, Bastiaens HJM, Biedron SG, Danailov MB, et al. (2010) High Harmonic Source for Seeding of Fermi@Elettra. J Proc FEL2010 262-265.

41. Lambert G, Hara T, Garzella D, Tanikawa T, Labat M, et al. (2008) Injection of harmonics generated in gas in a free-electron laser providing intense and coherent extreme-ultraviolet light. Nat Phys 4: 296-300.

42. Takahashi EJ, Hasegawa H, Nabekawa Y, Midorikawa K (2004) High-throughput, high-damage-threshold broadband beam splitter for high-order harmonics in the extreme-ultraviolet region. Opt Lett 29: 507-509.

43. Kojima Y, Eilanlou AA, Furukawa Y, Nabekawa Y, Takahashi EJ, et al. (2012) Material Survey for a Novel Beam Splitter Separating High-Order Harmonics from High-Average-Power Fundamental Pulses. J Appl Phys 51: 062601.

44. Palik ED (1985) Handbook of optical constants of solids, Volumes I, II and III. Academic Press, San Diego.

45. Luxel Corporation (2013) Private communication.

46. Gudat W, Kunz C (1979) In: Synchrotron Radiation. Kunz C, Volume 10, Springer: Berlin, Heidelberg 55-167.

47. Salières P, Christov I (2009) Macroscopic effects in high-order harmonic generation. In: Strong Field Laser Physics; Brabec T, Springer Series in Optical Sciences; Springer New York, 261-280.

48. Constant E, Garzella D, Breger P, Mével E, Dorrer C, et al. (1999) Optimizing High Harmonic Generation in Absorbing Gases: Model and Experiment. Phys Rev Lett 82: 1668-1671.

49. Dachraoui H, Auguste T, Helmstedt A, Bartz P, Michelswirth M, et al. (2009) Interplay between absorption, dispersion and refraction in high-order harmonic generation. J Phys B 42: 175402.

50. Seres J, Wobrauschek P, Streli C, Yakovlev VS, Seres E, et al. (2006) Generation of coherent keV x-rays with intense femtosecond laser pulses. New J Phys 8: 251.

51. Heyl CM, Güdde J, l'Huillier A, Höfer U (2012) High-order harmonic generation with μJ laser pulses at high repetition rates. J Phys B At Mol Opt Phys 45: 074020.

52. Takahashi E, Nabekawa Y, Otsuka T, Obara M, Midorikawa K (2002) Generation of highly coherent submicrojoule soft x rays by high-order harmonics. Phys Rev A 66: 021802.

53. Midorikawa K, Nabekawa Y, Suda A (2008) XUV multiphoton processes with intense high-order harmonics. Prog Quantum Electron 32: 43-88.

54. He X, Miranda M, Schwenke J, Guilbaud O, Ruchon T, et al. (2009) Spatial and spectral properties of the high-order harmonic emission in argon for seeding applications. Phys Rev A 79.

55. Samson JAR, Stolte WC (2002) Precision measurements of the total photoionization cross sections of He, Ne, Ar, Kr, and Xe. J Electron Spectrosc Relat Phenom 123: 265-276.

56. Link O, Lugovoy E, Siefermann K, Liu Y, Faubel M, Abel B (2009) Ultrafast electronic spectroscopy for chemical analysis near liquid water interfaces: concepts and applications. Appl Phys Mater Sci Process 96: 117-135.

57. Luxel Corporation (2014) Standard Filters.